Proc. of the European Safety and Reliability Conference (ESREL 2026)
Edited by José C. Matos, Paulo B. Lourenço, Michael Beer, Daniel Oliveira,
Edoardo Patelli, Hélder S. Sousa, Rui A. Silva and Monica Santamaria
 Published by Research Publishing, Singapore.
doi: 10.3850/ESREL2026061419_esrel26-p26469-cd

PINN-Based Online Monitoring Method for Sensor Drift

Jiyong Lee

Department of Nuclear Engineering, KAIST, Republic of Korea. E-mail: jylee2588@kaist.ac.kr

Jonghyun Kim*

Department of Nuclear Engineering, KAIST, Republic of Korea. E-mail: jonghyun.kim@kaist.ac.kr

Safe and stable operation of nuclear power plants (NPPs) relies on accurate and reliable instrumentation. Conventional sensor calibration in NPPs is performed manually at fixed intervals, which can overlook abnormal behavior between outages and increase maintenance costs due to unnecessary recalibration of healthy sensors. Online monitoring (OLM) addresses these limitations by assessing sensor health in real time during plant operation and enabling condition-based maintenance. Despite extensive researches on artificial intelligence-based OLM, many approaches require large training datasets and operate as black boxes, offering limited physical interpretability. This work proposes a sensor drift detection method based on a physics-informed machine learning that combines a long short-term memory (LSTM)-based autoencoder with a physics-consistency constraint derived from a governing physical equation. By embedding the physics constraint into the loss function, the proposed model promotes physically plausible reconstructions even with limited data, thereby improving drift-detection performance and enhancing interpretability. The suggested method can provide a stable, physically consistent framework for drift monitoring and offer a practical route to reliable and explainable sensor health monitoring in NPP instrumentation.

Keywords: On-Line Monitoring, Physics-Informed Autoencoder, Signal Validation, Sensor Drift

1. Introduction

Reliable instrumentation is essential to ensure the safe and stable operation of nuclear power plants (NPPs). To maintain instrumentation reliability, sensor performance is typically verified through testing and calibration (Hashemian 1995; Hashemian 2011). Conventional testing and calibration are generally conducted periodically through manual procedures during overhaul periods. Therefore, sensor health cannot be continuously assessed during plant operation, and abnormal conditions arising between maintenance intervals may remain undetected. In addition, manual calibration can lead to unnecessary calibration and maintenance costs because sensors operating normally may be recalibrated indiscriminately along with degraded sensors (Coble et al. 2012; EPRI 1998).

Furthermore, small modular reactors (SMRs) that have longer operating cycles and the transition to modular configurations have reduced spacing between instruments and potentially cause instrumentation interference (Cetiner et al. 2021; Ramuhalli et al. 2016; Kim and Kim 2023). With this light, online monitoring (OLM) has received increasing attention because it enables real-time assessment of sensor health during plant operation without any interference and, through signal validation, supports calibration during overhaul only for sensors that require it (NRC n.d.).

OLM methods can be classified into redundant and non-redundant approaches. The redundant approach utilizes multiple channels measuring the same physical quantity. A non-redundant approach estimates expected values using correlations and physical relationships among related variables (e.g., pressure, temperature, and flow rate) even in the absence of redundancy (Fantoni et al. 2003). Although the redundant approach is intuitive to implement, spillover may occur in multivariate prediction when degradation of a particular input sensor contaminates other sensor estimates, causing residuals to change

in a cascading manner. In addition, under common-cause drift (systematic bias), where multiple channels change in a similar direction due to the same cause, drift may be judged as normal, making anomaly identification difficult.

The non-redundant approach can generate expected values by leveraging constraints between different physical quantities (e.g., mass and energy conservation, equations of state, and valve or pump characteristics) even without redundancy in the same measured quantity. As a result, even if a single sensor drifts, physical-consistency provided by other variable sets can mitigate the propagation of contamination. However, typical data-driven methods are prone to extrapolation issues when the diversity of normal data is insufficient or when operating modes change, whereas model-based methods can be difficult to deploy in practice due to model complexity and plant-specific implementation constraints.

To address these issues, this study proposes an OLM algorithm based on a physics-informed autoencoder (PI-AE) for sensor drift detection. The proposed PI-AE exploits the reconstruction capability of an autoencoder under nominal conditions while incorporating a physics equation into the loss function during training to encourage physically consistent estimation even with limited data. The proposed algorithm is implemented and validated using pressurizer pressure signals using the software-generated data, and the results demonstrate that the PI-AE-based OLM approach provides a stable and physically consistent drift-monitoring framework, offering a practical pathway toward reliable and explainable sensor health monitoring for NPP instrumentation.

2. Method

This section presents a method of OLM for sensor drift detection in NPP process instrumentation. Typical data-driven monitoring models may suffer from degraded reliability during operating transients and may produce physically inconsistent reconstructions. To improve robustness and physical plausibility, this study proposes a PI-AE framework that integrates data-driven time-series reconstruction with a physics consistency constraint as illustrated in Fig. 1.

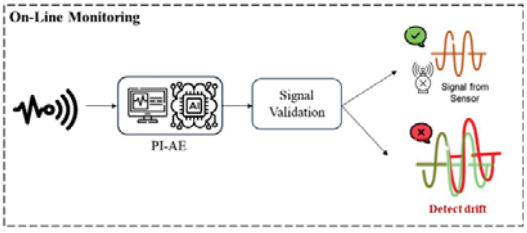

Fig. 1. PI-AE OLM

Real-time sensor measurements are continuously provided to a PI-AE, which reconstructs the corresponding sensor signals from the input sequence. A physics-consistency constraint derived from a governing equation is incorporated to promote physically plausible reconstructions. The PI-AE output is then used in signal validation, where the discrepancy between measured and reconstructed signals is quantified as reconstruction error (RE). Sensor drift is declared when RE exceeds a predefined threshold. Section 2.1 describes the PI-AE algorithm, and section 2.2 explains the signal validation.

2.1. *Physics-informed autoencoder*

The PI-AE combines a long short-term memory-based autoencoder (LSTM-AE) for multivariate time-series reconstruction with a physical-consistency constraint derived from a governing physics equation. The model is trained on nominal (healthy) data so that normal patterns are reconstructed with low error, whereas drifted signals are expected to produce larger reconstruction errors. For practical deployment using instrumentation-available measurements, state variables required by the physics constraint but not directly measurable (e.g., density) are treated as internal model variables and inferred from measurable inputs while being constrained by the governing equation.

2.1.1. *Long short-term memory-autoencoder*

Let $x(t) \in R^m$ denote an m-dimensional vector of measurable process variables at time t. Using a sliding window of length L, the input sequence is constructed as in Eq. (1).

$$X(t) = (x(t-L+1), \cdots, x(t)) \in R^{L \times m} \quad (1)$$

The reconstruction backbone of the proposed PI-AE is an LSTM-AE, which learns to compress and reconstruct ordered multivariate sequences. Specifically, the encoder LSTM maps the input sequence $X(t)$ into a latent representation $z(t)$, and

the decoder LSTM reconstructs the original sequence from the latent code according to Eq. (2).

$$z(t) = f_\theta(X(t)), \quad \hat{X}(t) = g_\theta(z(t)) \qquad (2)$$

The model is trained to minimize the discrepancy between the input and the reconstruction, typically using mean squared error (MSE). When trained on nominal (healthy) operation data, the LSTM-AE reconstructs normal patterns with low errors, whereas sequences containing abnormal behaviors such as sensor drift are harder to reconstruct and tend to yield larger reconstruction errors. The PI-AE outputs a reconstructed sequence $\hat{X}(t)$; for online monitoring, the reconstructed vector at the most recent time step, denoted by $\hat{x}(t) \in \mathbb{R}^m$, is extracted and used to compute a time-indexed monitoring indicator (reconstruction error). In this study, a standard LSTM-AE without the physics-informed constraint is also implemented as a baseline model to explicitly evaluate the performance improvement and training stability contributed by the proposed physics loss.

2.1.2. *Physics informed neural network*

Data-driven reconstruction models may generate physically implausible outputs, particularly during operating transients or when the training data do not sufficiently cover diverse operating conditions. To improve robustness and physical plausibility, the proposed PI-AE adopts the concept of PINN, which incorporates governing physical equations into the training process in addition to fitting observed data (Karniadakis et al. 2021). Unlike conventional data-driven approaches that minimize only prediction (or reconstruction) errors, PINN learning introduces a physics-consistency penalty that discourages solutions violating known physical laws. In a typical formulation, network outputs are substituted into a governing equation to compute a physics residual, which quantifies the degree of physical inconsistency. In the proposed PI-AE, physical consistency is enforced by defining a physics residual, denoted as $r_{\text{phys}}(t)$ which measures the violation of a governing physical equation G, as given in Eq. (3).

$$r_{\text{phys}}(t) = G(\hat{y}(t), \hat{s}(t)) \qquad (3)$$

where $\hat{y}(t)$ denotes reconstructed measurable variables relevant to the governing equation, and $\hat{s}(t)$denotes additional state variables required by the governing relationship. In practical NPP environments, some required variables may not be directly measurable (e.g., density). To maintain deployability using instrumentation-available measurements, the PI-AE is designed to infer such variables internally as auxiliary state estimates $\hat{s}(t)$from measurable inputs. These internal states are learned by minimizing the physics residual, thereby encouraging physically meaningful state estimation and physically consistent reconstruction. The physics loss is defined as a residual penalty as defined in Eq. (4).

$$L_{\text{phys}} = \frac{1}{N}\sum_{t=1}^{N} \| r_{\text{phys}}(t) \|_2^2 \qquad (4)$$

where Ndenotes the number of training samples and $\|\cdot\|_2$ denotes the Euclidean norm. In parallel, the reconstruction loss measures agreement between the input and reconstructed sequences using mean squared error (MSE) as in Eq. (5).

$$L_{\text{rec}} = \frac{1}{N}\sum_{t=1}^{N} \| X(t) - \hat{X}(t) \|_2^2 \qquad (5)$$

The PI-AE is trained by minimizing a weighted sum of the reconstruction loss and the physics loss as expressed in Eq. (6).

$$L = \lambda_{\text{rec}} L_{\text{rec}} + \lambda_{\text{phys}} L_{\text{phys}} \qquad (6)$$

where λ_{rec} and λ_{phys} are weighting coefficients. By jointly minimizing these terms, the PI-AE learns to reconstruct nominal multivariate sequences while discouraging violations of the governing physics, resulting in more robust and physically plausible reconstructions for online monitoring.

2.2. *Signal validation*

This section describes how the proposed PI-AE is used for OLM through signal validation (Tung et al. 2025). As illustrated in Fig. 2, streaming sensor measurements are pre-processed and fed into the PI-AE to generate reconstructed signals (expected values); the discrepancy between the measured and reconstructed signals is then quantified as the RE and evaluated against a predefined threshold (optionally with a persistence criterion) to classify sensor status in real time**.**

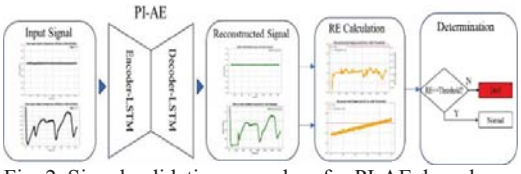

Fig. 2. Signal validation procedure for PI-AE–based OLM

Process variables have different scales and units, inputs are normalized prior to model use. In this work, variable-wise min–max normalization based on training data is applied, as defined in Eq. (7).

$$x_j^*(t) = \frac{x_j(t) - x_j^{min}}{x_j^{max} - x_j^{min}},\ j = 1,2,\ldots,m \quad (7)$$

where x_j^{min} and x_j^{max} are determined from the training dataset. The normalized vector $x^*(t)$ is then used to form the input sequence $X^*(t)$ for the PI-AE. Given an input sequence $X^*(t) \in \mathbb{R}^{L\times m}$, the PI-AE produces a reconstructed sequence $\hat{X}^*(t)$. For online monitoring, the reconstructed vector corresponding to the latest time step is denoted by $\hat{x}^*(t) \in \mathbb{R}^m$, enabling a time-indexed monitoring indicator that can be updated as new measurements arrive.

For thresholding in the original scale, the reconstruction error is defined as the discrepancy between the measured and reconstructed signals, as expressed in Eq. (8).

$$RE(t) = |x(t) - \hat{x}(t)| \quad (8)$$

During online monitoring, $RE(t)$ is tracked over time. Sensor drift is suspected when $RE(t)$ increases persistently, reflecting a growing mismatch between observed measurements and the model's learned normal pattern.

Sensor drift is declared when the reconstruction error exceeds a predefined threshold, as defined in Eq. (9).

$$RE(t) \geq \tau \Rightarrow \text{Drift detected} \quad (9)$$

Two decision modes can be employed depending on monitoring requirements: a static threshold mode for nominal operations, and a persistence-based condition mode for transient or emergency conditions. In safety-critical instrumentation environments, alarm thresholds may differ by operating regime because signal variability can change substantially during abnormal conditions and emergency transients.

3. Experiments

This section evaluates the proposed PI-AE–based OLM method using simulation data generated with MARS-KS. The experiments are designed to (i) train the PI-AE to reconstruct multivariate instrumentation signals while enforcing physics consistency through an embedded governing equation and (ii) assess online signal validation performance for sensor drift detection. Specifically, the PI-AE is trained on datasets representing normal operation and representative transient/emergency conditions, and drift scenarios (e.g., zero shift and span shift) are then injected to examine whether RE-based signal validation can reliably detect.

3.1. Data collection

To perform signal validation under normal and abnormal conditions, a dataset was generated using multi-dimensional analysis of reactor safety-kins standard (MARS-KS), a best-estimate thermal–hydraulic analysis code of NPPs. The dataset covers three operating conditions NORMAL, inadvertent opening of a steam generator atmospheric dump valve (IOSGADV), and main steam line break (MSLB):

- NORMAL: stable operating condition.
- IOSGADV: abnormal transient caused by unintended opening of the atmospheric dump valve.
- MSLB: emergency scenario involving rapid secondary-side depressurization and rupture of a main steam line with a large steam release.

For each condition, key event-driving parameters were varied to span a range of severities. Gaussian noise (σ=0.073) was added to the simulated signals to emulate instrumentation uncertainty. Furthermore, to simulate sensor degradation during the testing phase, synthetic drift scenario specifically zero shift and span shift—were generated and injected into the test datasets in accordance with the EPRI sensor drift classification framework (EPRI 2014). The dataset composition is summarized in Table 1. Out of 164 cases, 80% were used for training and

validation, and the remaining 20% were used for testing.

Table 1. Number of collected scenarios.

No	Scenario	Number of cases
1	NORMAL	30
2	IOSGADV	70
3	MSLB	64

3.2. *Input/output variables selection*

Inputs were chosen to (i) capture correlation with the monitored variable of interest under both normal and abnormal scenarios and (ii) ensure practical deployability by restricting candidates to variables measurable by plant instrumentation. In the PI-AE framework, the input and output variable sets are identical because the model reconstructs the same multivariate vector provided at the input. To quantify associations between the variable of interest and candidate process variables, Pearson and Spearman correlation analyses were performed for each scenario (de Winter, Gosling, and Potter 2016). Pearson correlation measures linear dependence between two variables and is defined in Eq. (10).

$$r_{xy} = \frac{\sum_{n=i}^{l}(x_l-\bar{x})\sum_{n=i}^{l}(y_i-\bar{y})}{\sqrt{\sum_{n=i}^{l}(x_l-\bar{x})^2\sum_{n=i}^{l}(y_i-\bar{y})^2}} \quad (10)$$

Spearman correlation evaluates monotonic relationships based on ranked values, providing a complementary measure when nonlinear behavior is present in process data, and is defined in Eq. (11).

$$p_{xy} = \frac{\sum_{n=i}^{l}(R(x_l)-\overline{R(x)})\sum_{n=i}^{l}(R(y_l)-\overline{R(y)})}{\sqrt{\sum_{n=i}^{l}(R(x_l)-\overline{R(x)})^2\sum_{n=i}^{l}(R(y_l)-\overline{R(y)})^2}} \quad (11)$$

For each scenario, variables satisfying the Pearson and Spearman correlation criteria $(0.90 \le p_{xy} \le 0.95)$ were screened as candidates. Variables that are not measurable in field instrumentation environments were then excluded to determine the final set. Through this process, 20 variables were selected as the final input/output variables for the PI-AE algorithm, as listed in Table 2

Table 2. List of input/output variables.

Variable	Component	Location
Thermal Power	Reactor power	-
Pressure	Pressurizer	-
Temperature	Steam Generator (SG)	A/B
Mass flow rate	Cold Leg	A-1, A-2/B-1, B-2
	Hot Leg	A/B
Water level	SG	A/B
	Pressurizer	-

3.3. *Physics equation selection*

To construct physics constraints applicable to pressurizer pressure estimation, four representative thermodynamic equations of state were considered as candidates, as listed in Table 3: the ideal gas equation, the Van der Waals equation, the Redlich-Kwong equation, and the Peng-Robinson equation. For each model, pressure values computed from the equation of state were compared with the pressurizer pressure data to evaluate scenario-wise applicability.

Table 3. Candidate physics equations.

Model	Physics equation
Ideal gas	$PV = nRT$
Van der Waals	$P = \frac{nRT}{v-b} - \frac{a}{v^2}$
Redlich-Kwong	$P = \frac{nRT}{v-b} - \frac{a(T)}{\sqrt{T}v(v+b)}$
Peng-Robinson	$P = \frac{nRT}{V-b} - \frac{a(T)}{V^2+2bV+b^2}$

Pressurizer pressure values computed from each equation of state were compared with the pressurizer pressure data obtained from MARS-KS. MSE and the coefficient of determination (R^2) were used as evaluation metrics. As listed in Tables 4 to 6, each candidate model was assessed under the NORMAL, IOSGADV, and MSLB scenarios to examine robustness to operating condition changes. Across scenarios, the Peng-Robinson equation provided the best overall agreement. In particular, the Peng-Robinson equation achieved an MSE of 0.001034 and R^2 of 0.997 in the IOSGADV scenario, and it also showed the best performance in the NORMAL and MSLB scenarios. Therefore, the Peng-Robinson equation was selected as the physics equation embedded in the PI-AE model.

Table 4. Performance evaluation results for the equation for NORMAL.

Model	MSE	R^2
Ideal gas	0.02533	0.991
Van der Waals	0.0053	0.98
Redlich-Kwong	0.0072	0.886
Peng-Robinson	0.0036	0.995

Table 5. Performance evaluation results for the equation for IOSGADV.

Model	MSE	R^2
Ideal gas	0.20771	0.677
Van der Waals	0.00425	0.99
Redlich-Kwong	0.00276	0.995
Peng-Robinson	0.001034	0.997

Table 6. Performance evaluation results for the equation for MSLB.

Model	MSE	R^2
Ideal gas	3.705	0.632
Van der Waals	0.02087	0.99
Redlich-Kwong	0.00646	0.995
Peng-Robinson	0.00097	0.999

3.4. *Training*

To ensure reconstruction stability and generalization across operating conditions, the PI-AE model was trained using the NORMAL, IOSGADV, and MSLB datasets. As illustrated in Fig. 3, The objective function was designed to jointly minimize both the data loss and the physics loss, where the physics-consistency term was computed based on the Peng–Robinson equation. The model was trained to compress multivariate inputs consisting of 20 sensor variables over a 30-time-step window and to reconstruct the original input sequence.

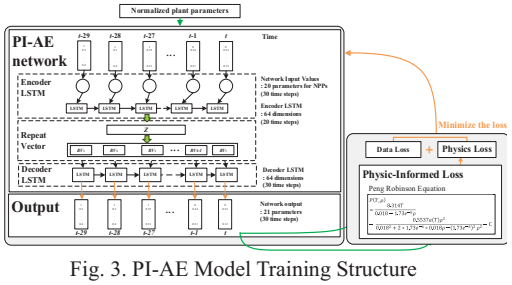

Fig. 3. PI-AE Model Training Structure

4. Results

During training, the validation datasets were monitored. As shown in Table 7, the agreement between the input signals and the reconstructed outputs was evaluated for each scenario using MSE, mean absolute percentage error (MAPE), and the coefficient of R^2. The results indicate that, across the NORMAL, IOSGADV, and MSLB scenarios, both training and validation R^2 values were close to 0.99, confirming that the model stably learned and reconstructed the dominant patterns of the input time-series signals.

Table 7. PI-AE validation performance

Model	MSE	MAPE	R^2
NORMAL	4.63E-05	3.90%	0.995
IOSGADV	3.3E-04	1.11%	0.999
MSLB	6.53E-05	5.08%	0.995

4.1. *PI-AE validation*

After training, the PI-AE model was verified using RE evaluation for each scenario. RE verification requires a drift-detection threshold, and for nuclear power plant instrumentation, these criteria may differ depending on whether the plant is in normal/abnormal operation or under emergency conditions. For NORMAL and IOSGADV: The instrument tolerance band was set to 0.18615 MPa, with a corresponding PI-AE drift detection threshold of 0.3. For MSLB: To reflect the large pressure variation in an emergency scenario, the instrument tolerance band was set to ±0.59294 MPa, with a corresponding threshold of 0.029. As shown in Fig. 4, verification was performed for the trained scenarios (NORMAL, IOSGADV, and MSLB). The RE remained within the specified threshold ranges, confirming that the model can classify the trained operating conditions as normal.

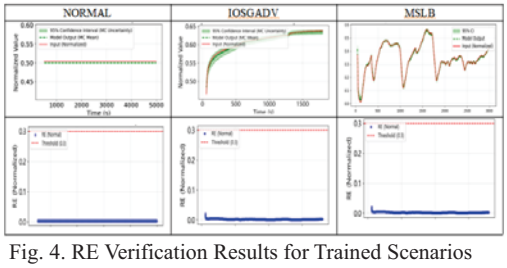

Fig. 4. RE Verification Results for Trained Scenarios

4.2. *Drift detection tests of the PI-AE*

This section evaluates the drift detection performance of the PI-AE online monitoring algorithm including Zero Shift, Span Shift (Forward/Reverse). The model was trained to achieve stable reconstruction and physical consistency across operating conditions (NORMAL, IOSGADV, and MSLB). As shown in Figs. 5 to 7, drift tests were performed to verify whether reconstruction-based monitoring can reliably detect gradual sensor bias over time, with emphasis on early detection capability and false-alarm behavior.

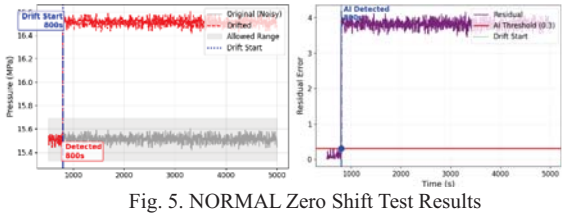

Fig. 5. NORMAL Zero Shift Test Results

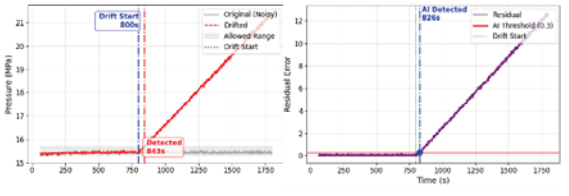

Fig. 6. IOSGADV Forward Span Shift Test Results

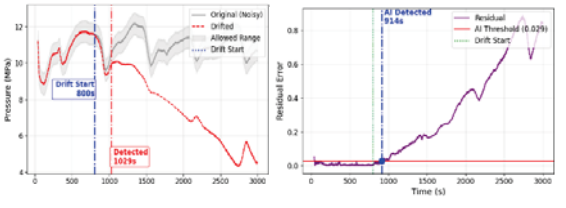

Fig. 7. MSLB Reverse Span Shift Test Results

Across all drift types and scenarios, RE increased after the drift injection and exceeded the threshold, confirming successful drift detection by the PI-AE. In addition, RE remained below the threshold before drift injection, indicating no false alarms in the nominal region. Notably, the PI-AE often detected drift earlier than the instrument-tolerance-based criterion. When Zero drift was injected at 800s, the signal-based drift decision defined using the predetermined signal threshold classified the sensor as drift at approximately 840s. In contrast, the PI-AE raised an alarm at approximately 816s as the reconstruction residual increased and exceeded the RE threshold, demonstrating earlier detection than the signal-based criterion. This difference demonstrates that RE-based monitoring provides earlier warning by identifying incipient inconsistencies with learned nominal behavior before the deviation becomes large enough to violate the instrument tolerance band. Overall, the results show consistent decision behavior across NORMAL, IOSGADV, and MSLB, with clear separation between normal and drift regions and persistent threshold exceedance after drift onset.

5. Discussion

A key contribution of the PI-AE framework is the explicit enforcement of physical consistency through a physics-loss term derived from the selected equation of state. This physics constraint contributes to performance improvement in two aspects. First, it suppresses reconstructions that minimize the data loss yet violate thermodynamic relationships, thereby promoting physically plausible reconstructions even during rapid operating transitions or under out-of-distribution conditions. Second, as shown in Fig. 8, compared with the baseline LSTM-AE, the PI-AE converges faster and reaches stable loss levels with fewer epochs. This behavior can be interpreted as the physics constraint acting as an inductive bias that restricts the solution space to physically plausible regions and stabilizes gradient updates by reducing the degrees of freedom during optimization, thereby facilitating convergence. This effect can be particularly pronounced when training data are limited.

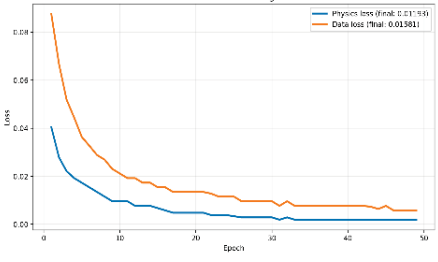

Fig. 8. Comparison of Training Loss Between PI-AE (blue) and LSTM-AE (orange)

6. Conclusion

This study proposed and evaluated a PI-AE framework for online monitoring of NPP instrumentation, focusing on sensor drift detection. PI-AE combines an LSTM-based autoencoder with a thermodynamics-based physics constraint to promote physically consistent reconstructions and improve robustness over data-driven models. A training and evaluation database was generated using MARS-KS simulations for the APR1400, covering normal operation (NORMAL) and representative transients (IOSGADV and MSLB). Sensor-drift datasets were additionally synthesized based on the EPRI drift classification framework, including zero shift, span shift, and combined drift patterns.

The results showed that PI-AE achieved high reconstruction accuracy across all scenarios and learned dominant multivariate time-series characteristics under varying operating conditions. The physics constraint also improved training efficiency, yielding faster and more stable convergence than the baseline LSTM-AE. RE served as an effective monitoring indicator: it remained within thresholds under nominal conditions and exceeded thresholds after drift injection for all tested drift types, indicating robust drift detection with a low false-alarm tendency in the evaluated cases.

Acknowledgement

This work was supported by the Innovative Small Modular Reactor Development Agency grant funded by the Korea Government (MIST) (No. RS-2023-00258052) and the Korea Institute of Energy Technology Evaluation and Planning (KETEP) grant funded by the Korean government (Ministry of Trade, Industry and Resources, MOTIR) (No. RS-2025-16063033).

References

Hashemian, H. M. 1995. On-line Testing of Calibration of Process Instrumentation Channels in Nuclear Power Plants: Phase 2, Final Report (NUREG/CR-6343). Washington, DC: U.S. Nuclear Regulatory Commission. November.

Hashemian, H. M. 2011. “On-line Monitoring Applications in Nuclear Power Plants.” Progress in Nuclear Energy 53 (2): 167–181. March.

Coble, J. B., et al. 2012. A Review of Sensor Calibration Monitoring for Calibration Interval Extension in Nuclear Power Plants. Report (OSTI PURL 1061413).

Electric Power Research Institute (EPRI). 2014. Guidelines for Instrument Calibration Extension/Reduction - Revision 2. Report 3002002556. Palo Alto, CA: EPRI.

Cetiner, S., et al. 2021. Testing of Instrumentation and Control Sensors and Cables for Advanced Reactors. Oak Ridge, TN: Oak Ridge National Laboratory (ORNL).

Ramuhalli, P., et al. 2016. “Robust Online Monitoring Technology for Recalibration Assessment of Transmitters and Instrumentation.” Slides presented at the U.S. DOE Office of Nuclear Energy Annual Review Meeting. October.

Kim, H., and J.H. Kim. 2023. “Long-term Prediction of Safety Parameters with Uncertainty Estimation in Emergency Situations at Nuclear Power Plants.” Nuclear Engineering and Technology 55 (5): 1630–1643.

U.S. Nuclear Regulatory Commission (NRC). n.d. “On-Line Monitoring for Calibration Extension: An Overview and Introduction to NUREG/CR-6895.” NRC Reading Room.

Fantoni, A., S. Figedy, S. Sanford, and K. Williams. 2003. “Methodologies for Sensor Validation and On-line Monitoring in Nuclear Power Plants.” Progress in Nuclear Energy.

Karniadakis, G. E., I. G. Kevrekidis, L. Lu, P. Perdikaris, S. Wang, and L. Yang. 2021. “Physics-informed Machine Learning.” Nature Reviews Physics 3: 422–440.

Tung, T.-Y., Y.-L. Hsu, S.-L. Huang, and C.-Y. (Ric) Huang. 2025. “Efficient Rectification Signal Validation for Optimal Functional ECO Patch Generation.” In Proceedings of the 62nd ACM/IEEE Design Automation Conference (DAC). June.

de Winter, J. C. F., S. D. Gosling, and J. Potter. 2016. “Comparing the Pearson and Spearman Correlation Coefficients across Distributions and Sample Sizes: A Tutorial Using Simulations and Empirical Data.” Psychological Methods 21 (3): 273–290.

Moran, M. J., H. N. Shapiro, D. D. Boettner, and M. B. Bailey. 2014. Fundamentals of Engineering Thermodynamics. 8th ed. Hoboken, NJ: John Wiley & Sons.